Available online at www.sciencedirect.com
ScienceDirect
International Journal of Rock Mechanics & Mining Sciences 45 (2008) 1025–1043
International Journal of Rock Mechanics and Mining Sciences
www.elsevier.com/locate/ijrmms

The 1873 collapse of the Saint-Maximilien panel at the Varangeville salt mine

P. Bérest[a], B. Brouard[b,*], B. Feuga[c], M. Karimi-Jafari[a]

[a]*LMS, Ecole Polytechnique, 92128 Palaiseau, France*
[b]*Brouard Consulting, 101 rue du Temple, 75003 Paris, France*
[c]*Geoderis, 1 rue Claude Chappe, 57075 Metz, France*

Received 5 July 2007; received in revised form 26 October 2007; accepted 31 October 2007
Available online 26 December 2007

Abstract

The 1873 panel collapse at the Varangéville salt mine (Lorraine, France) is described. Post-accident reports, as well as the experience drawn from neighbouring panels and mines, proved that pillars punched the marly layers on which they rested—a unique failure mechanism in the history of salt mines. The database on rock mechanical behaviour is relatively small, but it allows proposing credible values of the two most important mechanical parameters: floor cohesion and roof stiffness. Numerical computations confirm that the central pillar, despite its large horizontal dimensions, punched the floor and that large strains may have localized in the rock mass above the panel edge, allowing large-scale deformation of the roof and catastrophic evolution of pillar punching.

Keywords: Salt mine; Dilatancy; Mine collapse

1. Introduction

On October 31, 1873, the Saint-Maximilien panel of the Varangéville salt mine suddenly collapsed. The quake was felt in the town of Nancy, 10 km away from the mine. The panel had been evacuated in the morning, prompted by loud cracks and a fissure that developed in a building at ground level. Because it was payday, there were few workers in the mine, and casualties were relatively few.

The mine is still in operation, although, after this accident, mining methods drastically changed. Underground voids now are spread throughout an area larger than 3 km^2. However, this mine will be abandoned one day, and concerns have grown about the long-term evolution of man-made underground openings after they are abandoned, especially in densely inhabited areas in Europe. French mining authorities decided that the 1873 accident should be revisited to obtain better understanding of the mechanisms that led to panel collapse and to draw lessons that could be helpful in assessing the long-term stability of the remainder of the mine. This paper describes these efforts.

1.1. Observations made after the 1873 accident

A subsidence bowl had formed at ground level ([1] and Fig. 1). Shallow vertical fractures were visible along an outer circle (described as an ellipse in the 1873 reports) with a radius of 160 m and whose centre was at the head of shaft no. 1. This presented a clear sign of the effects of high tensile, horizontal stresses in this area. Along a concentric inner circle, approximately 80 m in radius, folds had formed, generated by high, compressive horizontal stresses. Inside the inner circle, the ground had remained flat and horizontal; it had subsided by 3.3 m. (This figure was measured at the shaft location.) Between the inner and the outer circles, the ground had taken a uniform inward slope that approximately was $\omega = 4/100$. The shaft was intact, but the shaft bottom was filled to a height of 18 m with various debris, including marls squeezed into the shaft when the shaft punched the underlying layers.

On November 1 and 2, several members of the mine staff and a mine inspector, Marie-Alfred Braconnier, who left

*Corresponding author.
E-mail address: brouard@lms.polytechnique.fr (B. Brouard).

1365-1609/$ - see front matter © 2007 Elsevier Ltd. All rights reserved.
doi:10.1016/j.ijrmms.2007.10.007

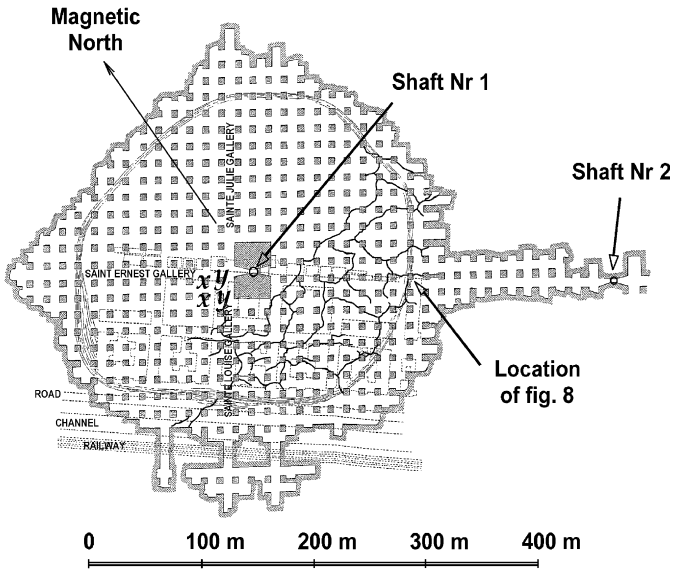

Fig. 1. Subsidence trough above the Saint-Maximilien panel as observed on November 1, 1873 (after [1]). Cracks along the outer ellipse, building locations at ground level, pillars and the irregular pattern of vertical mud-cracks at panel level also were reported.

detailed descriptions of the accident [1–4], came down shaft no. 2 to visit the collapsed panel. (Braconnier certainly wrote at least several parts of [4], whose author is unknown). The panel was located in the so-called 11th layer. Salt layers belong to the Lower Variegated Clay formation, or Lorraine Lower Keuper [5]. Geologists had divided the salt formation (from the salt roof, which is 80 m deep, to the mine, which is 160 m deep) into 11 salt layers separated by 10 marly layers, with thicknesses ranging from 0.5 to 3 m. The 11th salt layer is 20 m thick, and the purest salt is located at the base of this layer. Underneath the 11th layer is a 25 m (or slightly more) thick marly layer, which will be described in more detail below.

The panel was mined according to the room-and-pillar method. Openings were 5.5 m high, square pillars were 6 m × 6 m wide, and galleries were 8 m wide in the SW–NE direction and 9 m wide in the perpendicular direction, making the extraction ratio $\tau = 1-(6\times 6)/(14\times 15) = 82\%$ a ratio that was considered reasonable at that time. In the Saint-Maximilien panel, a 29 m × 40 m pillar was left at the centre of the panel to protect the access shaft. A description of the collapsed area was made by Braconnier (Fig. 2):

> Under the inner ellipse, at half-distance between the shaft no. 1 and the external contour of the panel, salt pillars had punched into the underlying marls. [Floor] marls had heaved to the roof of the galleries; the roof, which leaned towards panel centre, seemed to have mostly kept its initial strength; only fissures were visible. Between the inner and the outer ellipse (Fig. 2), no debris was spread on the ground. Floor slope was smooth and directed upwards to the shaft; roof slope was directed downwards. Pillars cores were split in several parts [2, p. 1].
>
> [Under the outer ellipse], large rock slabs had fallen and there were, at the galleries roofs, bell-shaped voids up to 3 m high (…) (Fig. 2). The walls of these voids were cut by opened fractures that followed the horizontal marly layers intercalated between the salt layers. It can be concluded that, on the mine contour, the rock mass was submitted to horizontal stresses which allowed debonding of the marly layers. [4, p. 625].

In 1855, the 4th salt layer, at a depth of 87 m, also had been mined (Fig. 3). The 1873 collapse generated no damage in this panel (except for a couple of fissures, at a 80 m distance from the axis of the shaft, from which a small amount of brine seeped out), which, together with the absence of severe damage in shaft no. 1, strongly suggests that the rock mass cylinder underneath the inner ellipse and above the "central pillar" came down as a rigid block, experiencing little or no deformation. A blind shaft and a gallery, of cross-section 3 m × 3 m, were dug out several years after the accident to link the 4th and 11th layers. This gallery allows observation of the rock mass a few metres above the external contour of the collapsed zone. Rock salt apparently is intact in this gallery, but small fractures, which allow air to circulate between the collapsed area and this gallery, can be seen on a 10 m long part of this gallery, exactly above the outmost galleries, suggesting that severe strains are likely to be localized in a circular crown under the zone where tensile cracks were observed at ground level. The kinematic compatibility of block displacements also suggests that a similar crown (in which large strains should be localized) exists under the inner ellipse where compressive folds were observed. However, no direct evidence supports this last assumption, except for the small fissures at the 4th layer panel edge (mentioned above).

It was noted that the salt pillars were almost intact. Minor damage was observed before collapse; after collapse, the pillars had not broken out, even at the panel edge, where the roof fell. Rock salt is a viscoplastic material, flowing even when submitted to small deviatoric stresses; strain rate, however, is a highly non-linear function of the applied load. In fact, a large reduction in pillar height, which could have been expected after 14 years, was not observed and, before the mine collapse, Braconnier asserted that "Rock salt is so competent and strong, so bereft of any fissure, its compressive strength is so large, that gallery width could be doubled, or pillar width could be made twice smaller, with no risk of roof fall" [7, p. 54], a statement that suggests that pillars were not deformed severely before the accident. However, before the accident and *a fortiori* after the accident, vertical fractures, 5 cm wide, could be seen in the pillars. Before the accident, most of them developed along vertical discontinuities in the salt (shown in Fig. 1) that are filled with marls and salt [8], see Section 5.2. Such discontinuities can be observed both in the 4th and 11th layers.

The absence of any water flow to the panel following panel collapse—a fact that remains true 130 years after the accident—also is remarkable. Mining often generates large stress redistribution in the rock mass—not large enough to

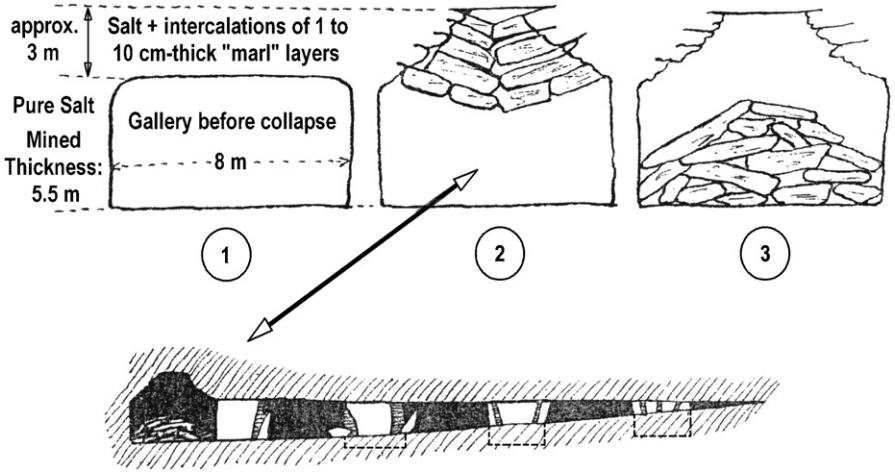

Fig. 2. Vertical cross-section of the three outmost galleries and sequence of events in the outmost gallery (after [2]).

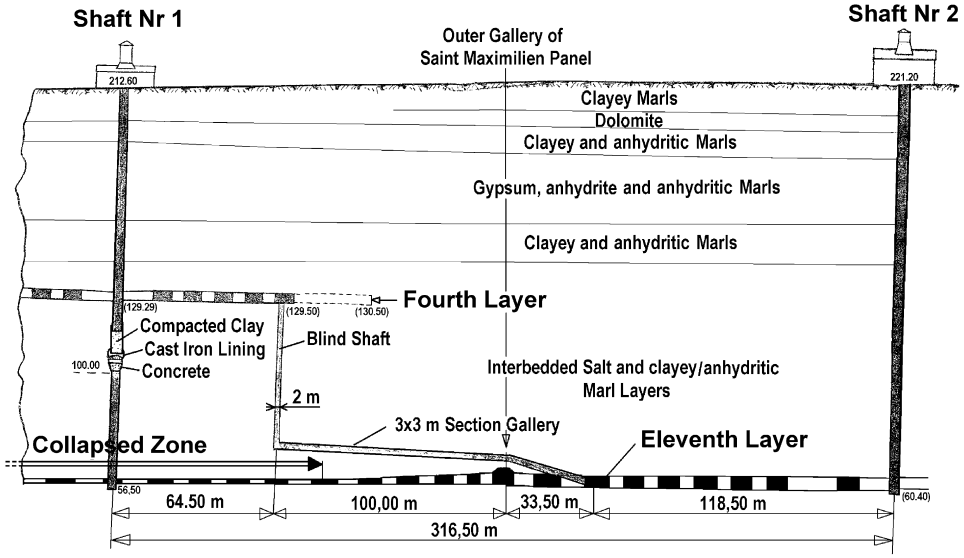

Fig. 3. Rock mass cross-section showing the 11th and 4th layers panels and the 3-m × 3-m gallery excavated after the accident (after [6]).

be a threat to mine stability, but large enough to provide underground water with an access to the mine through created or activated discontinuities [9]. In the case of the Saint-Maximilien panel, mechanical instability appeared, but no water flow was generated. Together with the absence of any visible vertical discontinuity in ground-level or mine-roof profile after the collapse, this fact suggests that no large-scale open fracture was created inside the rock mass.

1.2. Forerunners

It was said that mining was interrupted in the Saint-Maximilien panel a few hours before it collapsed, after a crack appeared in a building at ground level. In fact,

> For 15 days, at ground level, ground movements were revealed by failure, at many places, of cast iron pipes (…). For five to six months, galleries floor significantly heaved. In the Sainte-Julie gallery, we observed on October 20th that the floor had risen by 0.80 m[1]. A large number of pillars exhibited vertical fractures, from pillar top to bottom, whose aperture was 5 cm. The room of the water column device [which had been opened in the central pillar] could not be sustained any longer: it heaved by 6 mm a day. [[1] it even seems that galleries height shrank by up to 1.2 m, because of upward movement of the floor marls and also because pillars punched into the floor] [3, p. 2].

In addition, "Since 1868, it was noticed that pillars x and y (…) had fissured, and that marls at galleries floor swelled and weathered under the action of water and air" [4, p. 620]. (The four pillars x and y are located at the corner of the Saint-Ernest and Sainte-Louise galleries. Their distance to the shaft is less than 40 m; see Figs. 1, 4–6.)

Failure of the pipes and fissures in the pillars will be discussed later (Sections 5.3 and 4.2, respectively.) The reduction in gallery height by 80 cm (or more) in the Sainte-Julie gallery, which runs along one side of the protecting central pillar, and in other galleries also in the neighbourhood of the central pillar [4] is especially significant. The extraction ratio τ was more than 80%. This means that, on average, pillars must punch the floor by 64 cm, generating a 16-cm floor heave, to reduce gallery height by 80 cm, *except in an area close to the central pillar*, as even small punching by the central pillar generates the displacement of very large volumes of marls. It is impossible that a small number of square pillars punched the floor by 64 cm while neighbouring pillars experienced little or no punching. (The roof, submitted to large differential vertical displacements, then should have broken.) Hence, floor heave in the Sainte-Julie gallery results from the central pillar punching into the floor, an event that began before panel collapse.

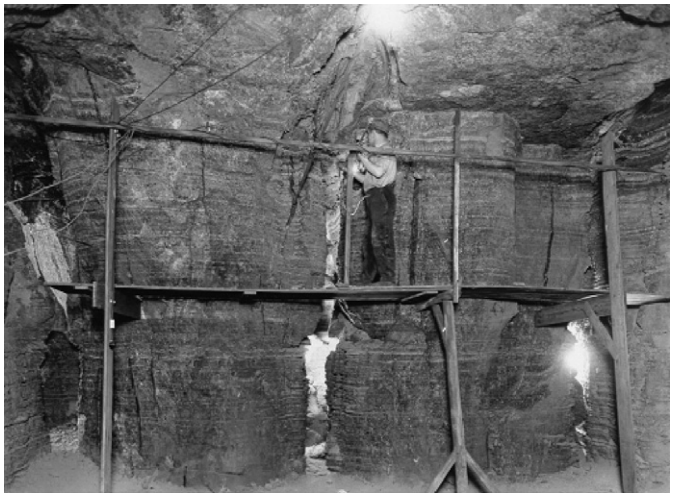

Fig. 4. Pre-cutting by water-jet in the Saint-Maximilien panel. This photo probably was taken several decades after the 1873 collapse (*Source*: CSME archives).

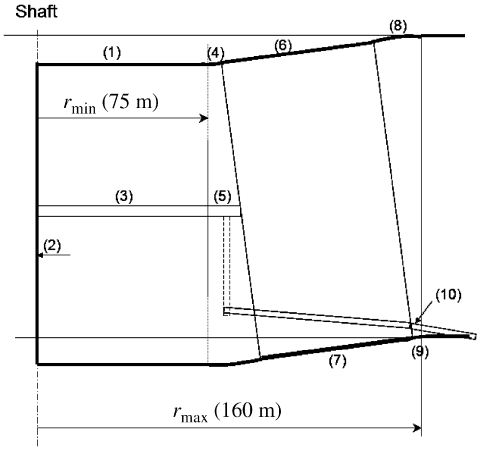

Fig. 5. Conceptual sketch of panel collapse.

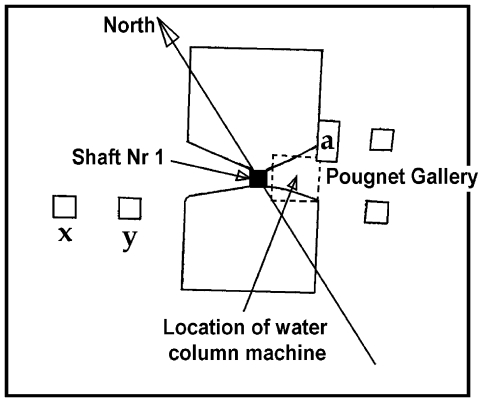

Fig. 6. Horizontal cross-section of the 29 m × 40 m central pillar. The dashed line shows where the water-column device room was located (after [3]).

The behaviour of the marly layer underneath the mine had drawn attention for a long time:

> This marly layer [at mine floor] probably is 20-m thick. In the uppermost part, it is extremely pure and must be cut by blasting. It is composed of grey-blue marls, extremely dense, containing irregular patterns of small reddish salt layers (…) and very strong pebbles, described as marls mixed up with salt and anhydrite [3, p.1].

Underneath this anhydritic marl crust are the much weaker "chocolate-brown" marls, whose thickness is a few metres. Both marl layers weather when in contact with water. Water was used to pre-cut the salt mass before blasting and was abundant in the mine. Unsaturated brine (concentration estimated to be 20° Baumé, or 250 g/l) seeped through the floor:

> After a 14-year long period of continuous mining, the amount of water that had seeped into the marls layer might have been notable (…) it should have leached out the salt layers and pebbles which are disseminated in the marls. Water should have hydrated anhydrite which, when transforming into gypsum, develops large breaking capacity. It should have weathered marls themselves, because of the oxygen dissolved in water, which had effects on the sulphides and organic materials which are contained in these pure marls. These three effects combine to weather the upper part of the marly layer which transformed into a spongy material [3, p. 1].

2. Some comments on salt-mine accidents

2.1. Mine flooding

The Saint-Maximilien collapse exhibits some unique features in the history of salt-mine accidents. The authors know of no other case involving salt pillars punching the floor. (This accident is common in coal mines or, for instance, in the trona mines in the Green River basin in Wyoming.) In [9] the case of a 500-m deep sylvinite panel is

described. A halite or sylvinite slab is left at panel floor, below which a generally massive soft and creep prone tachyhydrite layer can be found. The stiff roof/pillar system pushes pillars into soft tachyhydrite and floor heaves. In fact, most salt- or potash-mine accidents can be described by "mine flooding". Flooding of salt mines was a frequent accident during the 19th century. Despite considerable advances in exploration and production techniques, this type of accident remains quite common. Salt mines are very sensitive to water inflow: a small initial brine inflow may increase drastically as unsaturated brine leaches out the pathways through which it seeps into a mine, making further evolution dramatically rapid. (Several recent cases are described in [10]). In fact, mine flooding is sometimes a direct consequence of roof collapse, as in the Retsof case [11]; however, the dramatic features of this accident were caused by water flow into the mine rather than by the roof collapse itself. In the case of the Saint-Maximilien panel collapse, no water flow took place after the accident, strongly suggesting that no fracture was created.

2.2. Mine collapse

Potash mining in Germany has been affected by severe rock-bursts that generate quakes with magnitudes greater than 5 [12,13]. In the Stassfurt area, it is accepted that bending and failure of a competent layer, the Main Anhydrite of the immediate roof, is responsible for the dynamic character of collapses. In the Werra area, Minkley and Menzel convincingly assert that "the destruction phenomenon of thousands of pillars in just a few seconds" [12, p. 498] can be explained by the extreme brittleness of the mined ore (carnallitite). The 1873 collapse at Saint-Maximilien clearly is not due to bursting salt pillars: the height/width ratio of the central pillar is too small. While small square pillars are more slender, visual inspections made after the collapse proved that these pillars were split but kept their full height.

2.3. Cratering above solution-mined caverns

Hundreds of caverns have been solution-mined in the upper part of the Lower Keuper salt formation in which the Varangéville Mine was opened. Cratering takes place when the diameter of such caverns enlarges to become slightly smaller (say, 130 m) than cavern depth (say, 200 m). Two such cases are described in [14,15]. When leaching of these caverns was completed, the caverns had reached the top of the salt formation, stripping a marly layer that progressively weathered and fell to the cavern bottom. After several years, the immediate roofs of these caverns were a 6–8-m thick, 145-m deep competent layer, the Beaumont Dolomite, whose stiffness and strength are high. This layer bore the full overburden weight, and was supported partially by cavern brine pressure. Bending occurred, and severe tensile stresses developed both at the centre and at the periphery of the Dolomite plate, ultimately leading to roof failure, cavern collapse and formation of a sinkhole. However, even when the diameter is large, depressurising the cavern often is necessary to provoke pre-emptive collapse. (A similar failure mechanism was described in the case of sinkhole development above brine cavities in the Windsor-Detroit area [16].) In the Saint-Maximilien panel case, the Beaumont Dolomite layer is shallow (12 m below ground level, or 140 m above the mine). At such depth, the dolomite often is weathered by groundwater and cannot be considered as a competent layer. Significantly, no discontinuous vertical displacement (step) was observed at ground level above the Saint-Maximilien panel, in sharp contrast to the case of crater formation.

2.4. Neighbouring panels and Dieuze Mine

Comparison with neighbouring mines or panels can be more instructive. After the 1873 accident, mining methods in the Varangéville Mine drastically changed. A 20-cm thick salt slab was left at the floor, and soft water was no longer used to pre-cut the gallery face, protecting the marly floor layer from the weathering effects of air, water or brine. The gallery height still is 5.5 m, but the extraction ratio was decreased progressively, from 75% at the end of the 19th century to ultimately 52% in the currently mined panels. It is noted that few or no disorders were observed in these panels, even if some of them are more than a century old. (Salt pillar creep has been monitored for 30 years: the creep rate is slow, from 2 to 5 mm/year in areas where the extraction ratio is 75%, much less where it is 52%.)

A few dozens of kilometres from Varangéville, at Dieuze, a salt mine had been operated in the same salt formation from 1826 to 1864. The extraction ratio was similar (more than 80%), but the mine depth was smaller (120 m, instead of 160 m). Salt pillars rested directly on the same marly layer as in the Varangéville Mine. No water was used, and the mine remained stable during extraction. The mine was flooded in 1864. Flooding was the consequence of the collapse of a 60 m deep room connected to the mineshaft. A large brine pond had been created in this room; brine flowed down the shaft and filled the 120 m deep panel and the shaft [17]. In the 1990s, concerns were expressed that salt pillars and/or marly floor could have been weakened severely after having been kept in direct contact with saturated brine—as the floor had been during a 14-year extraction period in the Saint-Maximilien panel. In 2002, Geoderis, a French state agency in charge of post-mining issues, decided to drill a borehole to the mine. The borehole, and the sonar survey performed after the well hit the mine, proved that the mine had been preserved perfectly. The map drawn after the sonar survey measurement almost exactly matches the 140-year-old map drawn by the miners. The measured mine height had not changed, and the floor was perfectly flat. Weathering of the marly floor and punching into the floor by over-weighted pillars,

an event feared after the 1873 Varangéville collapse, clearly did not take place in the Dieuze Mine [17]. The reason for this probably can be explained by the following: mine depth at Dieuze is 3/4 that of Varangéville Mine; furthermore, after mine flooding was completed, the brine pressure in the 120-m deep mine lessened the effective weight of the overburden by a factor of 2, making the pillar load at Dieuze 3/8 of what it was at Saint-Maximilien. (Mine shape and size also are influential when load applied on pillars is assessed; Dieuze Mine was a rectangle and roof span was 130 m). Some experts also emphasize that Dieuze Mine was flooded by *saturated* brine, and that the anhydritic marl upper crust, which contains a significant amount of salt, was not weathered to the same extent as it had been at Saint-Maximilien, where *unsaturated* brine seeped into the floor [18]. This crust could have protected the much softer "chocolate-brown" underlying marly layer from the aggressive effect of brine.

From this comparison it can be inferred that two features are likely to explain the Saint-Maximilien collapse: on one hand, the mine depth and extraction ratio generated large loads on salt pillars and/or abutment; on the other hand, the marly layer beneath the pillars was weak and significantly weathered by water (or brine) seeping through the floor.

3. Collapse scenario

From this description, and additional comments made in the following paragraphs, a scenario of the collapse can be sketched. The marly floor was weak—and was made still weaker when the water used to pre-cut the pillars seeped into the floor. When the gallery opening generated additional loads on pillars, and provided a free surface for marls flow, the pillars began punching the floor. As long as horizontal dimensions of the panel were small, the panel roof remained stiff enough to prevent large vertical displacement of the pillars. When the panel enlarged, the roof span progressively increased, making the roof less stiff; as time went by, more water (or brine) seeped into the floor. Both phenomena allowed the pillars to punch deeper into the floor, which could not support a load larger than the low bearing capacity of the floor/pillar system. A large part of the overburden weight then was transferred to the abutments, and the pillar load remained relatively small. (A simple model of this is discussed in the appendix.) Large shear stresses developed above the panel edge, above which the salt experienced damage and softening, ultimately causing the roof stiffness to decrease abruptly. By 1873, large-scale rock mass deformation, which had been prevented by roof stiffness and strength, became possible, and full punching took place.

The central pillar, despite its large horizontal dimensions, punctured the marly floor that had been weathered by seeping water. A cylinder of ground above the central pillar and the closest small pillars, including shaft no. 1 and the 4th layer panel, approximately 160-m high and 150-m in diameter, dropped by 3.3 m, as a monolithic block, experiencing little or no deformation. No vertical fracture developed, but a 160-m high annulus dropped unevenly, with its external radius (at a, say, $r_{max} = 160$ m distance from the shaft axis) experiencing little or no vertical displacement and the internal radius (at a, say, $r_{min} = 75$ m distance from the shaft axis) subsiding by 3.3 m, preserving a smooth profile of both the ground surface and the panel roof. Largely deformed zones likely were localized in two (approximately) $L = 10$-m wide annuli above the outer and inner ellipse contours, respectively. These acted as "plastic hinges", allowing the salt mass and the overburden to bend and drop without experiencing fracturing.

This description is supported by the following evidences: (1) ground level remained flat inside the inner ellipse, (2) the shaft was intact, (3) the 4th layer panel was intact, (4) folds appeared at ground level, (5) two small fractures opened at the edge of the 4th layer panel, (6) ground remained flat between the inner and the outer ellipse, (7) panel roof remained flat, (8) tensile fractures opened at ground level, (9) roof fell in the outmost gallery and (10) small fractures are visible in the 3 m × 3 m gallery (see Fig. 5).

Fig. 5 gives a sketch of this. Strains and stresses can be assessed only through FEM computations, but simple estimations can be made. Let r, θ, z be cylindrical coordinates; the origin is at shaft head; z is oriented downward; and r_{min} and r_{max} are the radii of the inner and outer ellipse, respectively. Let ω be the slope of the ground between the inner and outer circles, $\omega \approx 0.04$. It is tempting to assume that $\varepsilon_{rz} = \omega/2$ (uniform shear) in the $r_{min} < r < r_{max}$ domain, but the uniform elastic stresses generated by such a strain field, or $\sigma_{rz} = 2\mu\varepsilon_{rz}$, are not consistent with what was observed at ground level (vertical fractures *and* folds). It is more realistic to assume that, in two annular domains, $r_{min} - L/2 < r < r_{min} + L/2$ and $r_{max} - L/2 < r < r_{max} + L/2$ a bending-like strain field developed and that the horizontal strain at ground level and at the panel roof, at r_{min} and r_{max}, is $\varepsilon_{rr} = +\omega H/2L$ or $\varepsilon_{rr} = -\omega H/2L$, figures that can explain the formation of tensile cracks and folds at ground level and roof fall at the panel edge. In this sketch, the domain $r_{min} + L/2 < r < r_{max} - L/2$ rotates as a block, consistent with observations made at ground level and in the mine (constant roof slope). Note that orthoradial strains (and stresses) are generated by such a rotation. Obviously, the situation was more complex in the actual multi-layered rock formation.

The objective of this study is to prove that this scenario is consistent with what is known from laboratory tests and field observations. Two parameters play a crucial role: floor cohesion (i.e., the bearing capacity of the floor/pillar system), and roof stiffness. These will be studied separately, as suggested, for instance, in [19].

4. Behaviour of the floor/pillar system

4.1. Floor-marl behaviour

The Varangéville Mine has been operated for more than a century, and miners consistently have reported that floor

marls dramatically weather when in contact with water (Section 1.2). It long has been recognized that this type of material exhibits a complex behaviour caused by strong interactions between water and rock matrix. Most marly layers soften when in contact with water, or even saturated brine. For instance, somewhat similar marls that compose the roof of the Hengelo salt caverns in the Netherlands were studied and reported on in [20], where the variety of possible micro-mechanisms that govern their behaviour is described.

The Varangéville marls first were studied from a geomechanical perspective in 1986 [21]. Mechanical properties were studied through different techniques. Test results were scattered, and defining a short-term failure criterion was not straightforward. In [21], a Tresca criterion, $C = 2\,\text{MPa}$, $\phi = 0^\circ$ for the *dry* and *shallow* (i.e., sampled in the immediate floor) material, is considered as being "safe". Creep tests also were performed on several samples; strain rates were not an increasing function of the applied stress, and varied haphazardly from one test to the other. It was noted that, in fact, samples swell as they take water, hiding some of the sample height reduction generated by creep. Inferring a definite constitutive law from these tests was impossible.

Samples also were submitted to a constant mechanical load (applied loads were from 2 to 6 MPa) and, after some time, were put in contact with saturated brine. Failure was obtained either immediately, or within a few days. In a recent Ph.D. thesis [18], tests performed on marls sampled from the same geological formation strongly suggest that hydration of anhydrite particles disseminated in the marls is the main mechanism explaining rock weathering—a phenomenon already highlighted by Braconnier 130 years ago (see Section 1.2)—rather than swelling of smectites that are present in the clayey phase, a mechanism that is inhibited when brine is saturated.

4.2. Water seepage through the floor

It is difficult to assess the extent to which the Saint-Maximilien floor marls had been weathered by water or brine before the panel collapse. Kinetics of water seepage is difficult to assess. (After the accident, water no longer was used in the mine, and few data are available.) However, it is obvious that, in certain zones, water could penetrate deep into the floor, under the upper anhydritic marl crust, down to the chocolate-brown marls, which are soft and especially sensitive to the action of saturated brine.

> Another circumstance helped the weathering of floor marls. Because of the general layer dip, which is 12 millimeter by meter toward N–NW in the eleventh layer, slots were dug out in the floor down to 2.5 m in some areas. Furthermore, the water column device and its basin had been set in a room excavated in the marly floor, partly below the large pillars protecting the shaft no. 1 [Fig. 6]. All these slots through the marls should have helped damp air or water action and should have lessened marls strength [3. p. 1].
>
> The height of one of the main galleries had been increased from 5.5 to 17 m, at the gallery face, and a big scaffolding had been set [it bore 18 iron pipes]. These pipes can be displaced freely; they are set to a rubber tube which provides soft water. This water runs down the wall and leaches rock salt [6].

From this, it can be inferred that the floor in the central part of the mine, where brine was collected from the rest of the panel, had weathered significantly:

> Marls weathering was made easier by the large number of cuts [in panel floor]. It is in the neighbourhood of the shaft that these cuts were more frequent and deeper; it also is in this specific area that marls had been submitted, for the longest period of time, to the influence of water and air. It is in this area that cohesion had vanished most completely and most deeply below rooms floors. Inside a circle whose radius was 60–80 meters, around the shaft, rock mass had become soft enough to allow pillars to punch the floor. At the periphery of the panel, however, floor had kept its full strength [4, p. 625].

However, it is difficult to distinguish fact from opinion in this statement. Indeed, it will be proven that, even when the cohesion of marls is uniform (i.e., evenly affected by water seepage into the entire mine floor), the central pillar punctures the floor.

4.3. Constitutive modelling of marls

It was decided to describe softened marls as a Bingham viscoplastic material with cohesion C and dynamic viscosity μ. This choice was based partly on the available database, which is small, and was partly heuristic: the existence of non-zero cohesion is able to explain why, in certain circumstances (in the Dieuze Mine case, for instance), punching does not take place. The average floor cohesion certainly was smaller than the short-term figure proposed in [21] for dry shallow material, $C = 2\,\text{MPa}$. Several figures were examined, and $C = 0.75\,\text{MPa}$ gave the best fit against field observations, as will be explained later. It would have been better to define cohesion as a function of depth, time and distance to the shaft, as the layer is not homogeneous and its strength changes with time because of water seepage. Because no precise data were available, it was considered that assuming homogeneous cohesion through the whole layer would give more conclusive results. (It will be proven that early floor punching by the central pillar takes place even when floor in the central area is not made softer than at the periphery of the panel.) The viscosity was still more difficult to select. Salt viscosity (at least at room temperature, when small loadings are applied [22]) typically is $\mu = 10^{17}\,\text{Pa s}$. It was decided to adopt a smaller figure, as it was known that the creep flow of marls is much faster than pillar salt creep, and $\mu = 10^{15}\,\text{Pa s}$ was selected. (Smaller values were tried, but they do not change the main

results significantly, and they make numerical computations tediously time consuming. After this study was completed, it appeared that the selected figure was not inconsistent with laboratory test results recently described in [18].)

4.4. Salt pillar behaviour

Rock salt is a viscoplastic material: in the long term, it flows even under very small deviatoric stress, and creep rate is a highly non-linear function of applied deviatoric stress. The Saint-Maximilien panel is at a depth of $H = 156\,\text{m}$, where the geostatic pressure approximately is $p = 3.5\,\text{MPa}$ When a mine is opened at such depth, relatively small deviatoric stresses—hence, slow creep rates—are expected to develop, except perhaps in the pillars. The extraction ratio in the Saint-Maximilien panel was more than $\tau = 80\%$, and, when it is assumed that no vertical load is transferred to the abutment, the average vertical stress in the pillar is $\sigma = p/(1-\tau) \approx 17.5\,\text{MPa}$ (tributary load), a relatively high figure. (In the following, compressive stresses are negative; "loads" borne by a pillar are positive.) In fact the actual pillar creep rate probably remained small for the following two reasons.

(1) The pillar is partly clamped into the salt roof. When the pillar deforms, horizontal stresses develop in the pillar, making the deviatoric stress smaller than the vertical stress, an effect that was described by several authors [23,24] and is stronger when the pillar is less slender.
(2) For the Saint-Maximilien panel, the vertical stress, which is borne by the pillars, must not be assessed using the tributary area assumption. In fact, it is slightly larger than the bearing capacity of the marl floor, which is small. A significant part of the overburden weight is transferred to abutments, and, consequently, pillar creep is slow.

As a whole, the viscoplastic behaviour of salt plays a minute role when the collapse mechanism is considered. However, mine creep closure was taken into account for numerical computations. The existing database described Varangéville salt as a Lemaitre–Menzel–Schreiner material (i.e., both steady-state and transient behaviours are described by the same power law):

$$\dot{\varepsilon}_{ij}^{vp} = K(\varepsilon^{vp})^m \frac{1}{(n+1)} \frac{\partial}{\partial \sigma_{ij}} \left(\sqrt{3J_2}\right)^{n+1}, \tag{1}$$

$$s_{ij} = \sigma_{ij} - \tfrac{1}{3}\sigma_{kk}\delta_{ij}, \quad e_{ij} = \varepsilon_{ij} - \tfrac{1}{3}\varepsilon_{kk}\delta_{ij}$$
$$J_2 = \tfrac{1}{2}s_{ij}s_{ij}, \quad \varepsilon^{vp} = \sqrt{\tfrac{3}{2}e_{ij}e_{ij}}. \tag{2}$$

4.5. Panel and pillar descriptions adopted for numerical computations

The actual panel contained a $29\,\text{m} \times 40\,\text{m}$ central protecting pillar (Fig. 6) and smaller $6\,\text{m} \times 6\,\text{m}$ square pillars (Fig. 1). The approximate external contour of the panel is a circle with a radius of 160 m (Fig. 1). Because we were not interested in the detailed mechanical behaviour of each pillar, but rather, in the global behaviour of the panel, a simplified axisymmetric description of the panel was adopted (see Section 5.1). One important constraint was to respect the overall extraction ratio—i.e., $\tau = 82\%$. The hundreds of actual square pillars were substituted in the model by 8 toric "pillars" separating 9 toric "rooms". The pillar and room widths are 2.87 and 13.18 m, respectively. The rectangular protecting pillar was substituted in the model by a circular pillar with a radius of 21.37 m. (This description of this "equivalent" axisymmetric mine, and of the opening chronology of the galleries, described in Section 6.2, are due to Gérard Vouille, to whom the authors are indebted.) The extraction ratio is the same in the model as in reality, which means that the loads supported by the pillars in the model are realistic. The same cannot be said of the ability of the pillar to "punch" into the floor on which it rests, as this ability depends on the size and number of the free surfaces (i.e., room floors) around the pillar. However, the difference is relatively small, as will be proven below.

4.6. Pillar punching

Because the salt-pillar creep rate is slow, a pillar can be considered to be a stiff body compared to the soft marly floor on which it rests. When an increasing vertical load, q, is applied on a pillar, the following is observed: when load is small, the load–displacement curve is linear, as both the pillar and roof behave elastically. However, the curve is no longer linear as soon as the viscoplastic criterion is met, somewhere inside the floor. This non-linearity remains discrete as long as the viscoplastic zone remains confined beneath the pillar. Eventually, when a viscoplastic zone large enough to isolate the pillar from the floor main body is created, the bearing capacity of the floor is reached, unconfined flow becomes possible, and the pillar punches the floor.

When the floor is a purely cohesive material ($C =$ cohesion of the soft marly floor), the onset of unconfined flow is characterized by the floor-bearing capacity—i.e., the critical ratio $\chi_c = q/C$. The Theory of Yield Design predicts that the onset of unconfined flow is independent of both the elastic constants and the viscosity of the floor. The case of a cylindrical pillar was discussed in [25]. When the floor is an infinite half-space, the onset of unconfined flow is independent of pillar radius; it is reached when the ratio between the applied axial load and the soil cohesion, q/C, approximately is $\chi_c = 6$. (When cohesion is $C = 0.75\,\text{MPa}$ the bearing capacity of the floor is $q = 4.5\,\text{MPa}$, a figure that is likely to be exceeded by the load transmitted to the floor by the pillar when the extraction ratio is larger than 80% in a 156-m deep mine.) In fact, at Saint-Maximilien, the soft floor is 25-m thick (or slightly more), and the bearing capacity of a circular pillar

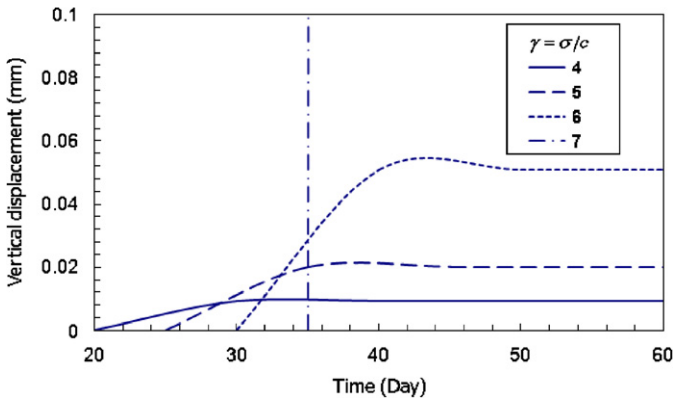

Fig. 7. Pillar vertical displacement (after the load is applied fully) versus time. Different vertical loads are applied to the pillar.

with a radius of 21 m can be suspected to be slightly larger than in the case of an infinite half-space. To verify the ability of the code to predict the bearing capacity of the pillars, numerical computations were performed.

Fig. 7 gives an example of this. A circular pillar is considered: floor cohesion is $C = 0.5$ MPa, its viscosity is $\mu = 0.3$ MPa year and the load is built up progressively at a 0.1 MPa/day rate to a final load of $q = 2$, 2.5, 3, 3.5 MPa, respectively. The final load is kept constant over several weeks. Non-linearity appears after some time (some viscoplastic zones develop before the bearing capacity is reached), displacements stabilize when q/C is smaller than 6, and unconfined flow takes place when $q/C = 7$. More precise computations prove that the (numerical) bearing capacity of an isolated circular pillar is $\chi_c = q/C = 6.6$.

The bearing capacity of a thin (i.e., whose width is much smaller than its radius) isolated torus (Tori mimic a set of square pillars equidistant from the shaft axis.) is likely to be close to the bearing capacity of an infinite strip, which is $\chi_c = q/C = 2+\pi$. Computations were performed and subsequently proved that the numerical bearing capacity of a torus was $\chi_c = q/C = 6$. Pillar-bearing capacity was expected to be slightly larger *in the mine*, because of possible interactions between neighbouring pillars, especially in the case of the central pillar.

4.7. Consequences

Selecting a relatively small cohesion of the marls floor has important consequences. As soon as the bearing capacity of the pillars is exceeded, the pillars punch the floor. If the vertical load applied on the pillar was kept constant, punching would stop only when the roof reaches the floor (or when compaction of the marls result in stiffening). In fact, pillar vertical displacement is partly prevented by roof stiffness: when pillars punch the floor, the roof bends and the vertical load applied by the roof of the pillar is made smaller.

The overburden weight is $p\pi R^2$. Pillars are able to support a small fraction of the overburden weight, or $(1-\tau)\chi_c C\pi R^2$ (approximately 1/4 of the total weight when $p = 3.5$ MPa, $\tau = 80\%$, $\chi_c = 6$ and $C = 0.75$ MPa). Hence a significant part of the overburden weight, or $[p-(1-\tau)\chi_c C]\pi R^2$, is transferred to the abutment. From this simple analysis it can be inferred that, when mine span (R) increases, the average vertical shear stress above the roof external contour is $\tau_{average} = [p-(1-\tau)\chi_c C]R/2H$, where H is the mine depth. This quantity increases with R, and damage above the mine contour is more likely when panel span increases. This simple inference will be proved to be correct (see Section 6.5). Note that when no punching takes place, $[p-(1-\tau)\chi_c C]$ tends to zero when mine span increases (each pillar bears its "tributary" load).

5. Roof stiffness

5.1. Salt stiffness versus roof stiffness

When overburden stiffness is considered, two notions must be distinguished. On one hand, the *elastic modulus of a salt sample* can be measured in the laboratory. It generally is assumed that the elastic modulus of Varangéville salt is $E = 26$ GPa, a figure that is in the range of variation of the elastic modulus of salt reported in the literature. On the other hand, the *stiffness of the roof* (which predominantly is made of salt) depends upon both mine size and the large-scale properties of the rock mass.

When the mine extent is very large (i.e., the horizontal dimensions are much larger than mine depth), the load borne by a pillar is close to the weight of the overburden, or p, divided by one minus the extraction ratio—i.e., $\sigma = p/(1-\tau)$, which is the definition of the "tributary" load. When mine extent is smaller, things are different. A simple model explains this notion. Let the mine be a flat cylindrical cavern of radius R (no pillar considered). The roof is a competent layer, has thickness η and elastic modulus E, and rests on the external abutment, which is assumed to be extremely stiff. In other words, the roof is a stiff plate clamped at the mine contour and bearing the weight of the overburden, or $p = \rho g H$; the plate inertia is I. Let $u = u(r)$ be the vertical displacement of the roof, and define roof stiffness (in MPa/m) as the ratio between the weight of the overburden and the vertical displacement of the plate centre:

$$p/u(0) = 64\mathrm{EI}/R^4 \tag{3}$$

then, roof stiffness is a (highly non-linear!) function of mine radius: when the horizontal dimensions of the mine are small, the roof is very stiff.

5.2. Roof stiffness assessment

There is no simple field test that allows assessment of the "large-scale" stiffness of the roof. The salt formation contains a large number of horizontal layers that have been described by many geologists (see, for example, [5]). The 1873 note [4] describes the depth and thickness of the 10

marly layers that separate the 11 salt layers from the salt roof to mine level (They range from 0.5 to 3 m in thickness.); however, at a smaller scale, many horizontal discontinuities also can be observed.

Braconnier [3] pointed out after his second visit (Section 1.1) that, in the 20-m thick 11th salt layer, there were, between the depths of 147 and 150 m, several thin marly layers whose mechanical significance is certain, as horizontal fractures developed inside these layers as a consequence of the collapse. Fig. 8, for example, is a photograph taken in the southern edge of the Saint-Maximilien panel, see Fig. 1 for exact location. (Note that, even in this area, where the room roof fell, the pillars were split but did not burst.) A large number of layers hanging from the roof clearly are visible.

Less frequent in a bedded-salt formation, many vertical discontinuities also are present; such discontinuities have been observed both in the 4th and 11th layers. Some of these discontinuities, as they exist in the 11th layer, are reported on the Saint-Maximilien panel map (see Fig. 1). A detailed description of these vertical fractures, which are filled with mudstone (marls), salt and anhydrite, and are organized according to a polygonal pattern (the reason that led to their being called "mud-cracks"), is given in [8], in which it is explained that these fractures were generated by shrinkage caused by large temperature differences between warm and cold periods during salt deposition. These vertical fractures also play a mechanical role. Before the collapse, it was observed that "Many pillars showed opened fractures, up to 5 cm wide, which run along the whole height of the pillar. They generally opened along the almost vertical clayey layers which cross through the 11th salt layer" [4, p. 620].

In the following, we will prove that these fractures were opened during extraction by the highly tensile horizontal stresses generated by marl flow under the pillars, when pillars punched the floor.

Fig. 8. Roof and pillar close to the external abutment in the collapsed Saint-Maximilien panel (*Source*: archives CSME).

5.3. Stiffness parameters

For numerical computations, a model of the roof that provides a realistic assessment of roof stiffness must be selected. For simplicity, the roof can be described as an elastic circular plate of radius R (Section 5.1), its stiffness being proportional to the product of an elastic modulus (E) multiplied by a bending inertia (I). If we select $E = 26$ GPa, and $I = \eta^3/12$, $\eta = 70$ m (thickness of the salt layer), then, when $R = 160$ m, the vertical displacement of the roof centre is $u(0) = 3.2$ cm when no pillar is left in the mine: clearly, the proposed roof stiffness is too high and must be reduced. (Subsidence of several decimetres occurred before the 1873 collapse; see Section 1.2 and below.) The modulus (E) can be made drastically smaller than the as-measured value, although such a reduction may appear to be somewhat artificial, as the as-measured modulus is well known. In fact, the salt formation contains not only salt, but also vertical mud cracks and numerous softer horizontal marly layers intercalated between the salt layers. Both contribute to a much smaller large-scale stiffness and lower strength. Thus, roof-bending inertia (I) can be modified by intercalating several such "soft" marly layers between thin salt layers. (When, instead of one plate, thickness η, one considers N plates, thickness η/N, separated by extremely soft and thin intercalated layers, the overall bending inertia of the N layers is $I_N = N(\eta/N)^3/12 = I_1/N^2$: inertia is divided by N^2.) This second option is more satisfying, as it is consistent with the geological description of the rock mass. However, meshing a large number of thin layers leads to a prohibitive number of elements and time-consuming computations: a compromise must be found. Three 3-m thick horizontal layers were set inside the rock mass at various depths, and the elastic moduli of the salt and marls were reduced significantly. Both moves led to softening of the salt roof (illustrated by Fig. 9). The panel is described as a cylindrical cavern, with radius of 160 m (No pillar is considered in this model; obviously, such a large "cavern" would not be stable, but we are interested here in roof stiffness rather than in the stability of such a virtual cavern.), and the vertical displacement of the roof is computed (the numerical model is described in Section 6.1) in three cases: (1) when the roof is *soft* (salt elastic modulus, $E = 1$ GPa; marl elastic modulus, $E' = 0.5$ GPa); (2) when the roof is *stiff* (salt elastic modulus, $E = 5$ GPa; marl elastic modulus, $E' = 1$ GPa); and (3) when the roof is *very stiff* (salt elastic modulus, $E = 26$ GPa; no marly layer is intercalated). The maximum displacement is reached at panel centre, or $u(0) = 74$, 28 and 10 cm, respectively. From this, it was inferred than only the "soft" roof should be able to push enough to allow pillars to effectively punch the floor, as explained below.

This was confirmed by the computations described later. Furthermore, before the accident, it had been observed that

> …since 15 days, at ground level, ground movements were revealed by failure, at many places, of cast iron

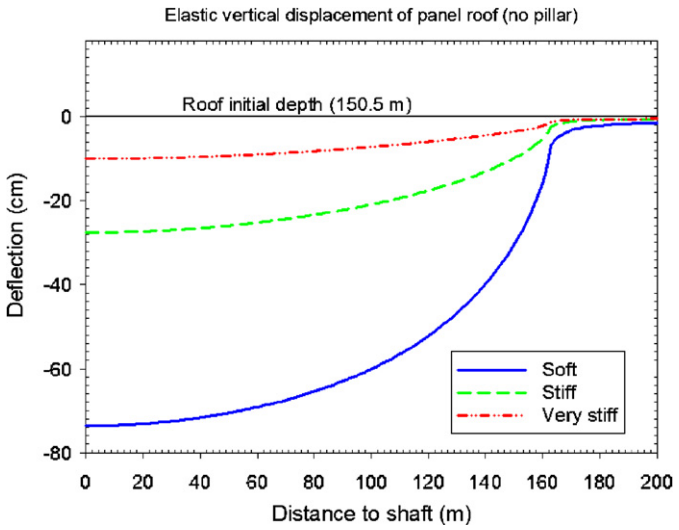

Fig. 9. Roof vertical displacement as a function of distance to the axis of symmetry.

> pipes (…). In the Sainte-Julie gallery, we observed by October 20th [1873] that floor had risen by 0.80 m [3, p. 2].

In [26] the following guidelines are proposed: "…The maximum permitted vertical subsidence for most buildings is 0.1 meter, and for some pipelines, it is 0.3 meter". From this, it can be inferred that vertical subsidence before panel collapse was several decimetres. Computations performed with the "soft roof assumption" (described above) showed that maximum subsidence at ground level was 32 cm in 1873 (before mine collapse), and much smaller when "stiff" or "very stiff" roofs were considered. The same computations proved that, when the "soft roof" assumption was selected, vertical displacement of the roof close to the central pillar was 40 cm and that the floor heaved by 50 cm, leading to a 90-cm reduction in room height, a figure consistent with field observations and providing some credibility to the "soft roof" assumption. However, rather than a realistic description of the roof, the selected model must be considered as a "black-box" which provides a correct assessment of the overall stiffness of the roof.

6. Roof–pillar–floor interaction

6.1. Reference model

Parameters selected for the reference numerical computations are described in Table 1. (Variants are discussed in Section 6.4) The model is axisymmetric: the rock mass is a 400-m thick cylinder with a radius of 300 m. At the model bottom, vertical displacements are zero, and no horizontal shear stress is applied. Because the constitutive behaviour of the materials whether is linear elastic or independent of the mean stress (except for the dilatancy criterion), it is convenient to compute the *additional* stresses generated by opening of the galleries: the rock mass is weightless, and a zero stress is applied to the lateral surface of the model (and on the horizontal surface, at the model top). The initial geostatic stress, which is isotropic, is added to the computed additional stresses during post-processing to get the actual stresses. The elements are 6-node triangles (3-node triangles may create some problems when constitutive behaviour predicts no volume variation during deformation). In most computations, 52,548 elements (105,434 nodes) are used.

6.2. Room creation

The panel was operated from 1859 (after shaft no. 1 was dug) to 1873 (before panel collapse took place). The rock mass model includes several viscoplastic materials (salt and floor marls), and galleries were opened progressively. In 1873, the rock mass certainly was still experiencing a transient mechanical phase; thus, modelling the history of gallery openings appeared necessary. It was assumed that the extraction rate (in m^3/year) had been approximately constant from 1859 to 1873 and the openings of 9 equivalent toric galleries would be simulated according to Table 2.

Opening of the last (no. 9) gallery was completed after 15 years. (At which time, the actual mine collapsed.) However, computations have been performed to include 25 years after shaft creation to get a better understanding of the long-term trends in mine evolution.

6.3. Panel behaviour

When the first galleries are opened in the model, at the neighbourhood of the shaft, pillars are cut and the average vertical load on each pillar (including the protecting pillar) increases from geostatic pressure ($p = 3.5$ MPa at a 150 m depth) to a larger figure that depends upon panel radius and roof stiffness. When the roof is soft and the cohesion of the floor marls is low (say, lower than $C = 1$ MPa), the floor-bearing capacity is exceeded (It is $\chi_c = 6$–7 times larger than floor cohesion.), and pillars punch the floor. This is true for both the central protecting pillar and the smaller toric pillars. This can be seen in Fig. 10, years 0–5. When a new pillar is added, the average vertical stress on the existing pillars increases rapidly and then slowly decreases to progressively reach the pillar-bearing capacity. Note that the vertical stress on the central pillar always remains smaller than the vertical stress on the toric pillars. The average vertical stress (averaged from the panel edge to the external radius of the model) also is computed in the external abutment: at this stage, this additional stress is small.

However, after 5 years, the maximum vertical displacement of the roof (Fig. 11) remains small (because the roof remains stiff as long as the panel diameter is small). Hence, vertical displacement of the pillars is hindered rapidly, because the roof is not able to "push" effectively upon pillars when vertical roof displacements approach their

Table 1
Rock mass properties

Rock name	Thickness (m)	Depth (m)	Density (kg/m^3)	Young's modulus (MPa)	Poisson's ratio	Constitutive law	Parameter set
Soil	12	0–12	2500	100	0.25	Elastic	
Dolomite	6	12–28	2700	45,000	0.23	Elastic	
Marls and sandstone	56	18–74	2500	5400	0.18	Elastic	
Salt	13	74–87	2300	1000	0.19	Lemaitre	Varangéville
Marls	3	87–90	2300	500	0.18	Elastic	
Salt	6	90–96	2300	1000	0.19	Lemaitre	Varangéville
Marls	3	96–99	2300	500	0.18	Elastic	
Salt	34	99–133	2300	1000	0.19	Lemaitre	Varangéville
Marls	3	133–136	2300	500	0.18	Elastic	
Salt	20	136–156	2300	1000	0.19	Lemaitre	Varangéville
Floor marls	25	156–161	2500	5400	0.13	Bingham	$C = 0.75$ MPa; $\mu = 3$ MPa/year
Substratum	100	181–281	2500	15,000	0.25	Elastic	

Table 2
Assumed chronology of the opening of the opening of the toric-equivalent galleries with origin of time = 1859

Gallery number	Horizontal cross-section (m^2)	Opening duration (years)	Opening start (years)
1	0.23×10^4	0.50	0
2	0.36×10^4	0.80	0.50
3	0.50×10^4	1.09	1.30
4	0.63×10^4	1.38	2.39
5	0.76×10^4	1.67	3.77
6	0.90×10^4	1.96	5.44
7	1.03×10^4	2.25	7.40
8	1.16×10^4	2.34	9.65
9	1.29×10^4	2.83	12.19

maximum values (i.e., the values reached if no pillar were left—a scenario that, incidentally, would lead to roof collapse).

New galleries are opened, and additional load is applied on the pillars (Fig. 10, years 5–15: an initial stress of 3.5 MPa must be added to assess the actual load on the pillars.), and, importantly, the roof stiffness decreases. (It is proportional to R^{-4} when the simplified model explained in Section 5.1 is considered, R is the radius of the panel.) Floor punching continues. The punching rate is determined by the panel-extraction rate and, to a lesser extent, by the viscosity of the salt and floor marls. Additional load is transferred to the external abutment. Had extraction ceased and had panel collapse not taken place (Fig. 10, years 15–25), further evolution would have been smooth. Because the viscosity of marls is relatively low, pillars rapidly reach a kind of equilibrium—they exactly bear their bearing capacity. Subsequently, a large part of the overburden weight is transferred to the external abutment, pillars stop punching the floor, the elastic roof bends significantly and is not able to apply a load larger than the pillar-bearing capacity. In fact, "equilibrium" is somewhat of a misnomer, as the viscoplastic salt roof and pillars continue to deform, but at a very slow rate.

Returning to earlier evolution, pillars push on the underlying marls that are expelled toward the free surfaces (i.e., gallery floors), and the gallery floors heave. Because the volume of the marls remains constant, the roof displacement/floor heave ratio equals the pillar area roof area ratio, which is $\tau/(1-\tau) \approx 4$, except when the galleries are close to the central pillar or external abutment, whose punching provides large volumes of marls for upheaval into the floors of neighbouring galleries. Fig. 11 displays the roof and floor displacement after 15 years (i.e., when the actual panel collapsed). The roof, which had an initial depth of 150.5 m, dropped by 40 cm on the axis of symmetry, slightly more in gallery no. 1, and progressively less when one moves to the external abutment. Pillars punch the floor (by 38 cm for the central pillar) and the floor heaves in the galleries (by 40 cm in gallery no. 1, less for the other galleries). (If one considers the central pillar plus the first gallery, the local extraction ratio is close to $\tau = 50\%$, and the floor heave equals the roof descent.) Heave is slightly smaller at the gallery centre than close to the pillars, as the vertical flow of the marls takes place close to the pillars, except for gallery nos. 1 and 9, because the volumes of marls expelled by the central pillar or the external abutment are quite large. The reduction in gallery height is the quantity the miners could observe: computations predict a 90 cm height reduction after 15 years in gallery no. 1 (80 cm and more had been observed in the Sainte-Julie gallery; see Section 1.2). The abutment also punches the floor (in the model). This computed effect is likely to be unrealistic, because in the actual mine, weathering of the marls preferentially took place in the central part of the mine, a phenomenon that is not accounted for in the model.

Fig. 12 shows a more detailed description of the displacement field in the first and second galleries. Roof displacements are identical in the two galleries, but the floor heave is much larger in the first gallery, as explained above. Under the first pillar, the flow is roughly symmetrical: displacements are directed both toward

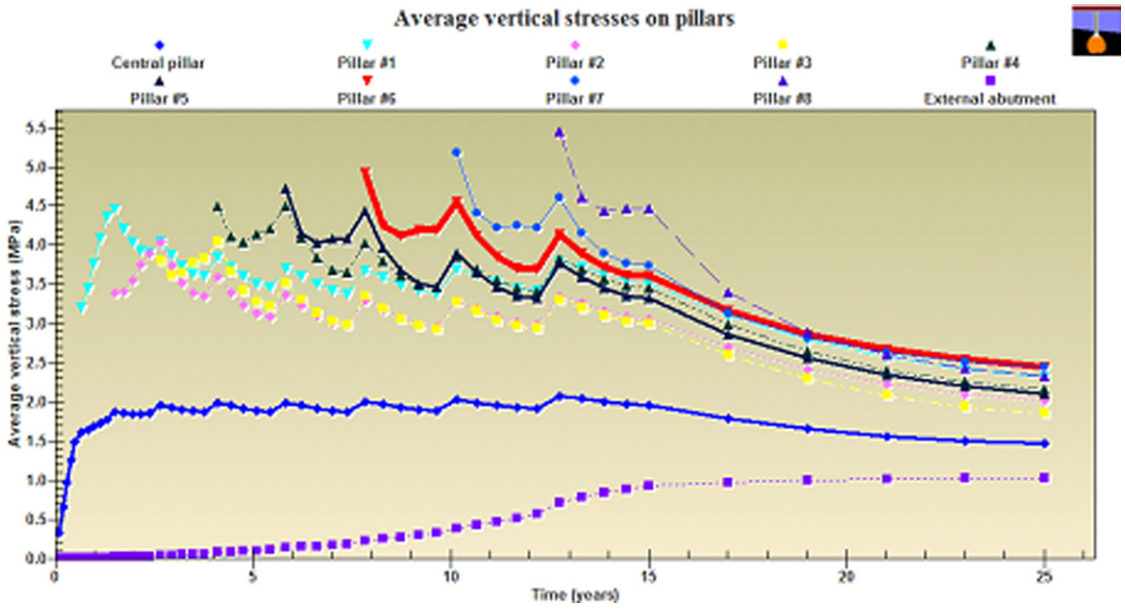

Fig. 10. Additional vertical loads on the pillars and external abutment as a function of time. A 3.5 MPa initial geostatic stress must be added to obtain the actual stress.

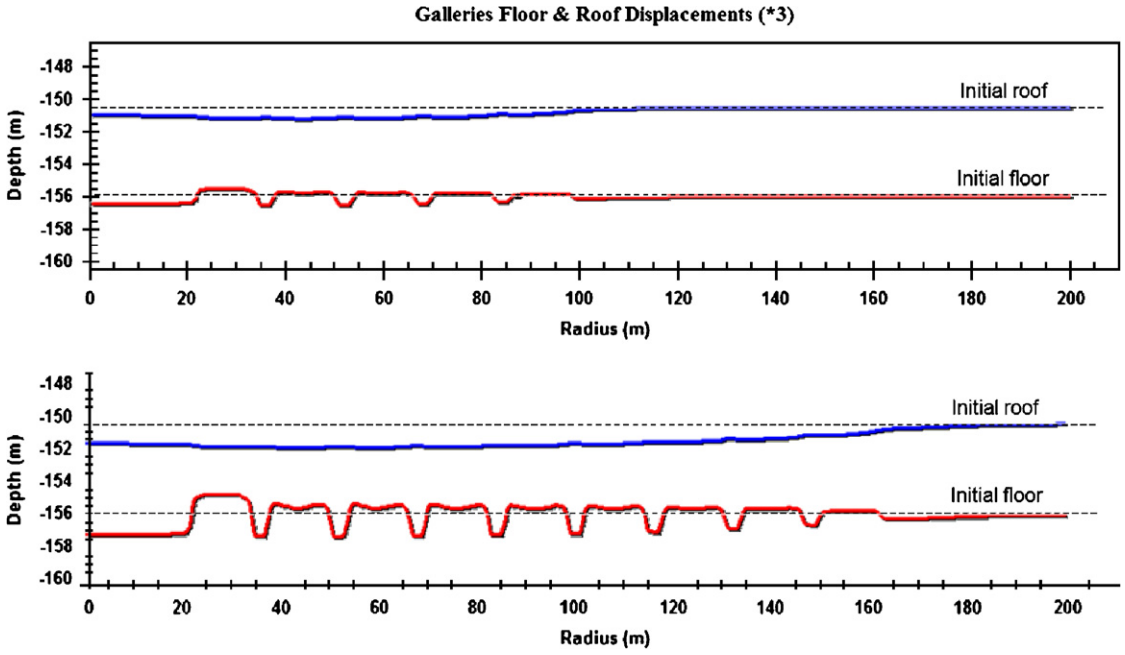

Fig. 11. Vertical displacements of the roof and floor after 5 years (above) and 15 years (below). Vertical displacements were multiplied by a factor of 3.

the inner and outer rooms that are separated by the pillar. (The same is true for all the other pillars, except for the outermost pillar, no. 8: in this specific area, marl flow is influenced deeply by the neighbouring external abutment.) The pillar base is pulled outward in the region closer to the outer gallery and inward in the region closer to the inner gallery: because a pillar is a stiff body (when compared to the soft floor), tensile horizontal stresses are generated at the base of the pillar. This can be seen in Fig. 13.

The upper part of pillar no. 6 partly is clamped into the relatively stiff salt roof, and horizontal compressive stresses develop, as horizontal expansion of the pillar partially is prevented. (The sixth pillar was selected because it is roughly at panel mid-span.) Conversely, tensile stresses develop in the lower part of the pillar as underlying marls flow inward and outward to the 6th and 7th galleries, respectively. In the actual mine, these stresses resulted in the opening of vertical fractures, preferentially following the marl-filled vertical slots that cross through the pillars.

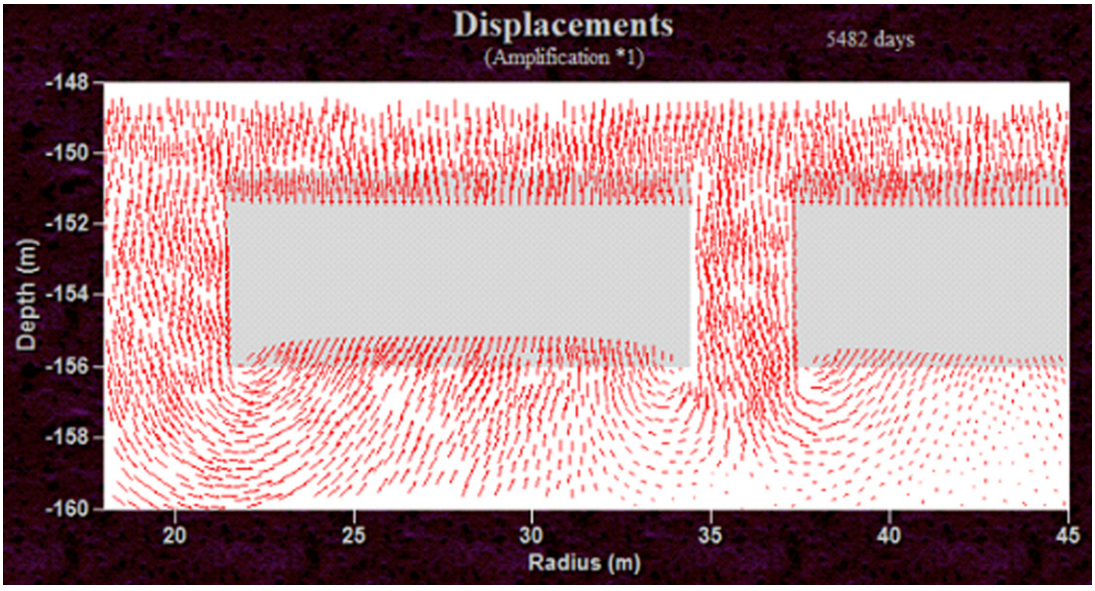

Fig. 12. Displacement field in the first and second galleries after 15 years.

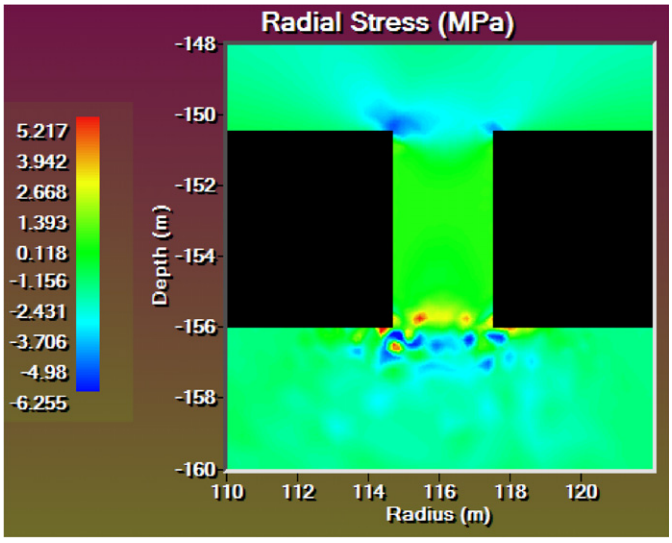

Fig. 13. Radial stress distribution at year 15 in the sixth toric pillar.

At both the roof and floor of each room, vertical tensile stresses develop. (In fact, small vertical compressive stresses are generated in a thin layer at the room floor, as proved by the equilibrium condition, $\sigma_{,z}+\rho g=0$.) In the gallery most remote from the central pillar, large compressive horizontal stresses develop in the upper and outer corners, an effect that is similar to what is observed in a bending plate.

6.4. Variants

The same computations have been performed considering various values of marl cohesion (keeping the "soft roof" assumption). When floor cohesion is $C=1$ MPa or 1.25 MPa (instead of $C=0.75$ MPa, as in the reference model), the average vertical loads on the pillars follow exactly the same trend as in the reference model: they slowly converge to pillar-bearing capacities, which are proportional to floor cohesion. Height reductions in the first galleries after 25 years are 74 and 25 cm (instead of 105 cm in the reference model). Because the actual height reduction in the Sainte-Julie gallery certainly was more than 80 cm, the choice of $C=0.75$ MPa is the best fit. When the cohesion is $C=2$ MPa, the computed average vertical load on the pillars is $\sigma=9$ MPa, a value smaller than the bearing capacity of the floor, which is χ_c $C=12$–13 MPa, and the gallery height variation after 25 years is 35 mm. Punching does not take place when floor cohesion is $C=2$ MPa, a figure that fits the "dry"-marl case. (After the 1873 collapse, water was not used for salt extraction, and a salt slab was left on the gallery floor, preventing weathering of the marls: punching did not occur.)

A stiffer roof also was considered. (The moduli of the salt and marls were made larger, and the floor cohesion was $C=0.75$ MPa, as in the reference model.) The average vertical stresses after 25 years are the same as those in the reference model. This is expected, as they are proportional to floor cohesion. However, during the 15-year initial transient phase (when the galleries are being excavated), these stresses are higher than in the reference model. Roof vertical displacement and floor heave are smaller by a factor of 2 (approximately). For instance, vertical displacements at the base of the central pillar are 44 and 21 cm, respectively. If there were no pillar, the vertical displacements of the roof would be 74 and 28 cm, respectively. In other words, equilibrium is reached when the vertical stress applied on the pillars equals the floor-bearing capacity, the roof deflection

being half-way from what it would be were no pillar present.

6.5. Failure

If no failure criterion were introduced in the model, mechanical evolution would remain smooth. After room creation stops, the system gradually converges towards an "equilibrium", as described above (Fig. 10, years 15–25). However, such equilibrium clearly cannot exist *in reality* when the panel reaches a large enough size, because pillars are able to bear only a small fraction of the overburden weight, whose main part is supported by the abutment, in which increasing vertical shear forces develop. There exists a panel radius above which failure must occur.

We know that several areas experienced severe disorders during the collapse. The roof of the outermost gallery fell, increasing gallery height by 3 m. This clearly was the effect of intense horizontal compressive stresses developing in this area as the roof leaned to the floor. It is suspected that two "hinges" formed under the inner ellipse (where a fold appeared at ground level) and the outer ellipse (where tensile cracks formed), and that large strains were localized in these (approximately) 10-m large, 150-m high zones (see Fig. 5). It is reasonable to assume that tensile cracks also appeared below the inner ellipse, close to the central pillar, but we have no direct evidence of this, as access to the central area was impossible after the panel collapsed. Some of this damage is a *consequence* of panel collapse; other parts of the damage are a *cause* of the collapse. In fact, the collapse can be initiated by sudden loss of cohesion in the panel floor or by rapid reduction in roof stiffness. A sudden loss of floor cohesion cannot be excluded completely—if it were, then the roof must be assumed to have been extremely soft, to allow rapid floor punching by the pillars as soon as floor lost cohesion, but this is difficult to believe, as floor weathering seems to have been a quite gradual process.

The rapid loss of roof stiffness is a more attractive option, but roof failure in the outermost gallery (compressive failure) or in the galleries located below the inner ellipse (tensile failure) is not able to change roof stiffness drastically. (For example, the fall of a 3-m thick roof slab does not change drastically the overall salt overburden thickness, which is 70 m.) Furthermore, when such a mechanism is accepted, it is difficult to believe that no precursory sign of imminent roof failure had been visible in the panel before collapse (none was reported). It is more tempting to attribute the loss in roof stiffness to a more generalized phenomenon affecting a large volume of salt: the formation of wide shear bands in which strain localization occurs. For this reason, a "dilatancy" criterion (i.e., onset of diffuse damage) was used. The criterion proposed in [27] for Cayuta (New York) salt was adopted, but the criterion was modified to take into account the existence of multiple weakness surfaces in the Varangéville salt mass and to better highlight the possible effects of dilatancy. The criterion can be written as (compressive stresses are negative)

$$\mathrm{FOS} = \frac{D_1|I_1/\sigma_0|^n + T_0}{(\sqrt{3}\cos\psi - D_2\sin\psi)}\Big/\sqrt{J_2} > 1,$$
$$3\psi = \arcsin\left[-\frac{3\sqrt{3}J_2}{2J_3^{3/2}}\right], \quad (4)$$

where T_0 is the rock tensile strength, FOS is the factor of safety (no dilatancy when FOS > 1), $\sigma_0 = 1$ MPa is a reference stress, ψ is the Lode angle, I_1 is the mean stress, and J_2 and J_3 are the second and third invariants of the deviatoric stress tensor, respectively. No tensile test was performed; the rock tensile strength was inferred from the cohesion and the friction angle in the low stress domain [27]. This criterion has the same general shape as the Hoek and Brown criterion, for instance; but a "compressive" triaxial state of stresses (the intermediate stress is larger than the average stress, $\sigma_3 < I_1/3 < \sigma_2 < \sigma_1 < 0$) and an "extensive" state of stress ($\sigma_3 < \sigma_2 < I_1/3 < \sigma_1 < 0$) are distinguished. The following values of the parameters were selected: $n = 0.693$, $D_1 = 0.5$ MPa, $D_2 = 0.524$, and $T_0 = 1$ MPa. (The parameters values are the same as in [27], except for D_1 and T_0, which were 0.773 and 1.95 MPa, respectively.)

Results of the computation are displayed in Fig. 14. The existence of the 4th layer panel was taken into account. The three pictures show the progression of the "dilatant" zone after opening of the 7th, 8th and 9th galleries, respectively. A continuous dilatant zone, extending from the panel edge to the salt top, formed during excavation of the 9th gallery. The formation of a zone below the opened cracks visible at ground level, in which large strain development becomes much easier, is an assumption supported by these results. However, some observations should be considered; these are discussed below.

6.6. Some comments on the "dilatancy" criterion

Dilatancy was observed in many rocks, including rock salt samples [28–35]. This must be distinguished thoroughly from sample failure. Dilatancy is characterized by an increase in sample volume—even though the applied stresses are compressive. The dilatancy criterion is a definite combination of stresses for which dilatancy appears [FOS = 1 in Eq. (4)]. Dilatancy is accompanied by drastic permeability increase, a drop in wave speed, and increase in acoustic emission. It generally is explained by the development of micro-cracks throughout the sample. A constitutive law for dilatant salt (in which healing also is taken into account) is proposed in [36]. The Kachanov theory of damage is used: the constitutive law keeps the same general form in the pre-dilatant and dilatant domains; when micro-crack density increases, however, instead of the actual stress that applies on any actual area, a fictitious "effective" stress, applied on the salt matrix (hence, larger than the actual stress) is taken into

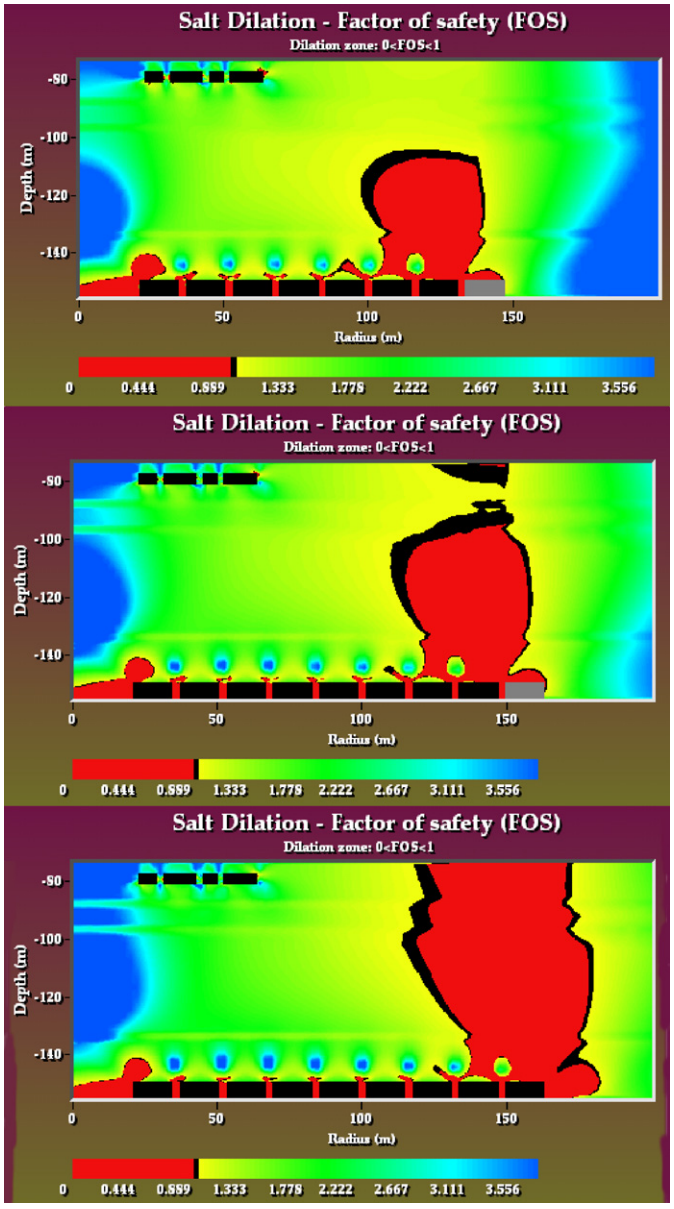

Fig. 14. Progression of the zone in which the dilatancy criterion is met during excavation of gallery nos. 7–9.

consideration inside the dilatant domain. More simply, dilatancy implies faster inelastic strain rates and material softening in the "dilatant" zone.

The dilatancy criterion commonly is used to design safe salt caverns [37–39]. The cavern and cavern pressure are designed in such a way that dilatancy should not appear (or appear in a very small volume of rock). For this reason, the Factor of Safety is computed, but the somewhat complex "dilatant" behaviour often is not taken into account fully.

In [40], an attempt was made to use the notion of dilatancy to explain the anomalous behaviour of a salt mine. The Weeks Island Mine is a two-level room-and-pillar mine in which the levels are 163 and 224 m deep, and the extraction ratio is $\tau = 55\%$. Two sinkholes, the first in 1992, appeared above the edge of the mine. This was an unexpected event, as the mine, which had been stable during mine operations, had been converted to an oil storage facility in 1981. It contained pressurized oil, which was thought to make the mine even more stable than it had been during the salt-extraction period. It was proved that a dilatant zone developed above the edge of the mine [40], providing some explanation for its otherwise puzzling evolution.

The onset of a continuous dilatant zone above the edge of the mine in the numerical model of the Saint-Maximilien panel after opening of the 9th gallery—i.e., immediately before the actual collapse of the panel—is a tentative explanation of roof softening (development of a dilatant zone made roof stiffness suddenly much smaller) causing the 1873 sudden panel collapse.

7. Conclusion

A numerical model was created of the mechanical behaviour of the Saint-Maximilien panel of the Varangéville salt mine before it collapsed. The panel floor is described as a viscoplastic cohesive material, and the panel roof stiffness is moderate. Both assumptions are supported by the mechanical behaviour database (which is small) and available geological descriptions. The model correctly accounts for the large reduction in gallery height in the central part of the panel, early punching of the floor by the central pillar, significant subsidence before panel collapse, the opening of vertical fractures crossing the pillars, and the slow vertical creep rate of the pillars. It predicts the likely softening of a large vertical strip in the salt formation above the panel edge when the horizontal dimensions of the panel are large. Softening may lead to the formation of a "hinge" above the panel edge, followed by the formation of a second hinge above panel mid-span; hinges drastically reduce roof stiffness and allow the central pillar to puncture the marly floor abruptly. This last part of the scenario (formation of plastic hinges) is tentative. Computations involving more sophisticated constitutive behaviour of salt ("post-dilatant" behaviour) could confirm the credibility of that part of the scenario. A large extraction ratio above a weak panel floor and additional loss of floor cohesion due to the use of water in the mining process are the two main factors explaining the collapse, which exhibits some unique features in the history of salt-mine accidents.

Acknowledgements

This study was made possible by a grant from Geoderis, the French state agency in charge of post-mining issues, which authorized publication of this paper. The Compagnie des Salins du Midi et des Salines de l'Est (CSME) kindly authorized the reproduction of photographs from the company archives, and Emmanuel Hertz provided useful comments. Gérard Vouille's help was instrumental with regard to the panel modelling, and he corrected several mistakes contained in an earlier version

of this paper. Jean Salençon and Alain Pecker provided helpful insights regarding the assessment of pillar-bearing capacity and dynamic effects. Special thanks to Kathy Sikora.

Appendix A. Simple model

In this appendix, we compare the mechanical behaviours of two circular panels. Panel radius (R), extraction ratio (τ) and roof bending stiffness (EI) are identical. The two floor/pillar systems are distinct: in the first case, the behaviour of the floor/pillar system is linear elastic: pillar height reduction is a linear function of the load applied on the pillar. "Soft" behaviour of the system is selected. (The difference with the "plastic" case is pronounced even more when the system is stiffer.) In the second case, the behaviour of the floor/pillar system is plastic: pillars punch the floor as soon as the applied load on the pillar reaches the floor-bearing capacity.

More precisely, the overburden is described as a thin elastic plate, whose bending stiffness is EI. Polar coordinates are used, and $u = u(r)$ is the vertical displacement of the plate. The mined salt layer, together with the marly layer on which it rests, are described as an elastic body: when a vertical load $\sigma = \sigma(r) > 0$ is applied on the salt layer, the resulting displacement is $u = \sigma/G$. For simplicity, it is assumed that the same relation holds for a pillar cut in this salt layer.

Before extraction, a vertical load, p (geostatic pressure), is applied uniformly to the plate, which remains horizontal. Extraction takes place: the panel radius is R, and the extraction ratio is τ. An additional vertical displacement, or u, results from the additional load generated by extraction.

In the abutment, $r > R$, the following relation holds:

$$\mathrm{EI}\Delta\Delta u + \mathrm{Gu} = 0, \tag{5}$$

where Δ is the Laplacian operator—i.e., $\Delta u = u_{,rr} + u_{,r}/r$.

In the panel, extraction results in an additional tensile load $-p$ applied to the room roof (i.e., below the plate). It is equivalent to an additional compressive stress $+p$ applied above the plate on a τ fraction of the panel horizontal area. On an $(1-\tau)$ fraction of the panel horizontal area (i.e., on the pillars), the following two cases must be distinguished.

In the elastic case, an elastic relation holds, $\sigma = \mathrm{Gu}$ and

$$\mathrm{EI}\Delta\Delta u - \tau p + (1-\tau)\mathrm{Gu} = 0. \tag{6}$$

In the plastic case, the bearing capacity is reached, the additional load is $\gamma_c C - p$, and

$$\mathrm{EI}\Delta\Delta u - p + (1-\tau)\gamma_c C = 0. \tag{7}$$

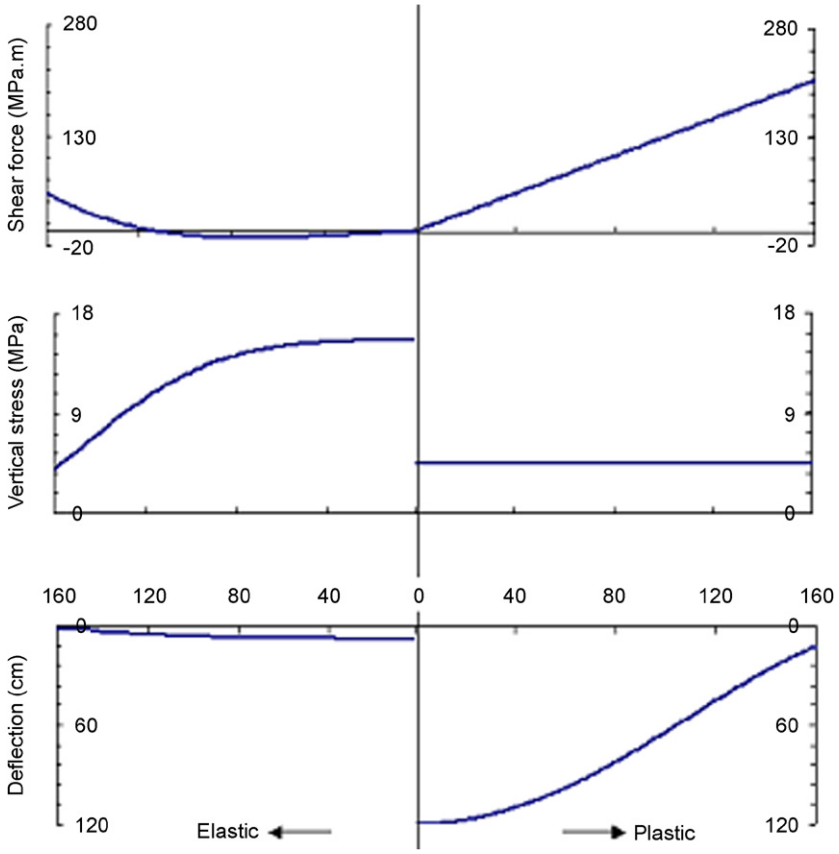

Fig. 15. Roof deflection, applied stress and shear force assuming an elastic (left) and plastic (right) panel floor as a function of the distance to panel axis of symmetry.

If one sets $l^4 = EI/G$ and $m^4 = EI/(1-\tau)G$, the solutions of (5) and (6) are $u = Aker(r/l)+Bkei(r/l)$ and $u = \tau p/(1-\tau)G + Lber(r/m)+Mbei(r/m)$, respectively, where the Kelvin functions ber, bei, ker and kei are the real and imaginary parts of the solutions of the equation $\Delta u+iu = 0$. The solution of (7) is a polynomial function, $u = (p-(1-\tau)\gamma_c C)(r^4+Pr^2+Q)/64EI$. At the panel edge, or $r = R$, displacement, slope, bending moment and shear force must be continuous—i.e., the displacement $u = u(r)$ and its three first derivatives with respect to r must be continuous. These four conditions allow computation of the constant coefficients A, B, L, M or A, B, P, Q in the solutions of (5), (6) and (7).

The following values of the mechanical constants were selected: $p = 3.5$ MPa, $\tau = 80\%$, $EI = 4.5 \times 10^7$ MPa m^3 (This figure was selected because it predicts a vertical displacement $u(0) = 0.75$ m for a plate with a radius of 160 m when the extraction ratio is $\tau = 1$ and the plate is clamped to the abutment.), $G = 200$ MPa m. (This figure is low and yields large pillar deformation. When the additional load on a pillar is 10 MPa and the pillar height is 5 m, its height reduction is 25 cm. Such a large value is an attempt to take into account the ability of rock salt to accumulate deformation when a period of time lasting several years is considered.) Results of the computations are shown in Fig. 15.

The following two cases were considered:

(a) Elastic behaviour (pillars not able to punch the floor)—The maximum vertical displacement is small (4 cm); conversely the average load on the pillars (more than 14 MPa at the centre of the panel) is close to the theoretical "tributary" load, or $\sigma = p/(1-\tau) = 17.5$ MPa. A small fraction of the overburden weight is transferred to the abutment, and the shear force at the panel edge is relatively small. These conclusions could be strengthened should stiffer pillar behaviour be considered.

(b) Plastic behaviour (pillar loads reach the bearing capacity of the floor and punching occurs)—The vertical displacement is large (more than 1 m; remember that, in this model, the plate is not clamped to the abutment, which behaves elastically), and pillars support a relatively small fraction of the tributary area. Conversely, a fraction of the overburden weight is transferred to the abutment, and the shear force and the bending moment (not represented) at panel edge are large.

The first model can be called "tributary": a large part of the overburden weight is supported by the pillars, and attention is drawn to pillar failure, the likeliest collapse mechanism. Conversely, in the second model, pillars support a relatively small fraction of the overburden pressure, and large shear forces and bending moments develop at plate edge. Formation of a hinge in the plate above the panel edge leading to roof failure is a credible collapse mechanism.

References

[1] Braconnier MA. Mine inspector first report on the collapse of the Varangéville-Saint Nicolas salt mine, Nancy (1er rapport de l'ingénieur des mines sur l'effondrement de la mine de sel gemme de Varangéville-Saint Nicolas, 2 Novembre 1873), unpublished, 1873 [in French].

[2] Braconnier MA. Mine inspector second report on the collapse of the Varangéville-Saint Nicolas salt mine, Nancy (2ème rapport de l'ingénieur des mines sur l'effondrement de la mine de sel gemme de Varangéville-Saint Nicolas, 3 Novembre 1873), unpublished, 1873 [in French].

[3] Braconnier MA. Mine inspector third report on the collapse of the Varangéville-Saint Nicolas salt mine, Nancy (3ème rapport de l'ingénieur des mines sur l'effondrement de la mine de sel gemme de Varangéville-Saint Nicolas, 4 Novembre 1873), unpublished, 1873 [in French].

[4] Unknown author. A note on the collapse of the Varangéville-Saint Nicolas (Meurthe-et-Moselle) salt mine. (Note sur l'effondrement de la mine de sel gemme de Varangéville-Saint Nicolas (Meurthe-et-Moselle)). Annales des mines, 7ème série, Tome IV, 1873. p. 613–27 [in French].

[5] Marchal C. The Keuper salt formation of Lorraine-Champagne and associated formations. Geometrical study. Genetical implications. (Le gîte salifère keupérien de Lorraine-Champagne et les formations associées. Etude géométrique. Implications génétiques.) Sc. De la Terre, Nancy, mém. No. 44, 2 volumes, 1983 [in French].

[6] Dautréaux A. Saint-Nicolas salt mine—a note on the 1873 October 31 mine collapse. (Mine de sel de Saint-Nicolas—Note sur l'effondrement de la mine du 31 Octobre 1873. Service des Mines (subdivision de Meurthe-et-Moselle)), unpublished, December 23, 1969 [in French].

[7] Braconnier MA. Mineral Wealths of the Meurthe-et-Moselle Department (Richesses minérales du département de Meurthe-et-Moselle). Nancy: Husson-Lemoine and Paris: Dunod; 1872 [in French].

[8] Robelin C, Bonijoly D. Sedimentary discontinuities in the Triassic salt formation at Varangéville, Meurthe-et-Moselle. (Les discontinuités sédimentaires de la série salifère triasique de Varangéville (Meurthe-et-Moselle)). Rapport BRGM-SGN R 31 834, Octobre 1990 [in French].

[9] Rothenburg L, Carvalo Jr ALP, Dusseault MB. Performance of a mining panel over tachyhydrite in Taqari-Vassouras potash mine. In: Wallner M, Lux KH, Minkley W, Hardy Jr RH, editors. Proceedings of the sixth conference on the mechanical behavior of salt. London: Taylor & Francis; 2007. p. 305–14.

[10] Bérest P, Brouard B, Feuga B. Dry mine abandonment. In: Bérest P, editor. Proceedings of the SMRI fall meeting. Kansas: Wichita; 2003. p. 9–37.

[11] Van Sambeek LL, Gowan SW, Payment KA. Loss of the Retsof salt mine: engineering analysis. In: Geertman RM, editor. Proceedings of the eighth world salt symposium, Salt 2000. The Hague, Amsterdam: Elsevier; 2000. p. 411–6.

[12] Minkley W, Menzel W. Local instability and system instability of room and pillar fields in potash mining. In: Hardy RH, Langer M, editors. Proceedings of the third conference on mechanical behavior of salt. Clausthal-Zellerfeld, Germany: Trans Tech Publishers; 1996. p. 497–510.

[13] Minkley W, Mühlbauer J, Storch G. Dynamic processes in salt rocks—a general approach for softening processes within the rock matrix and along the bedding planes. In: Wallner M, Lux KH, Minkley W, Hardy Jr RH, editors. Proceedings of the sixth conference on mechanical behavior of salt. London: Taylor & Francis; 2007. p. 295–304.

[14] Buffet A. The collapse of Compagnie des Salins SG4 and SG5 drillings. In: Proceedings of the SMRI fall meeting, Rome, 1998, p. 79–105.

[15] Jeanneau V. The sinkhole of the cavity LR 50/51 in La Rape Area, a case history. RHODIA Company. In: Proceedings of the SMRI fall meeting, Nancy, 2005. p. 9–24.
[16] Rothenburg L, Dusseault M, Mraz DZ. A methodology for rock mechanics design of brine fields based on case histories of sinkhole formation in Windsor-Detroit area. In: Cristescu ND, Hardy RH, Simionescu O, editors. Proceedings of the fifth conference on mechanical behavior of salt. Clausthal-Zellerfeld, Germany: Trans Tech Publishers; 2002. p. 389–92.
[17] Feuga B. Old salt mine at Dieuze (France) revisited 150 years after being abandoned. In: Proceeding of the SMRI fall meeting, Chester, UK, 2002. p. 114– 28.
[18] Boidin E. Interactions between rocks and brines in the context of mines and caverns abandonment. (Interactions roches/saumures en contexte d'abandon d'exploitations souterraines de sel). PhD thesis, Inst Nat Polytech Lorraine, February 2007 [in French].
[19] Board M, Damjanac B. Development of a methodology for analysis of instability in room and pillar mines. In: Stephansson O, editor. 2003 Swedish rock mechanics day conference. Stockholm: SveBeFo; 2003. p. 1–22.
[20] Bekendam RF, Oldenziel CE, Paar WA. Subsidence potential of the Hengelo brine field (Part I)—physico-chemical deterioration and mechanical failure of salt-cavern roof layers. In: Proceedings of the SMRI fall meeting, San Antonio, 2000. p. 103–17.
[21] Vouille G. Varangéville mine, mechanical behaviour of floor marls when put in contact with brine. (Mine de Varangéville, Comportement mécanique des marnes du mur en présence de saumure). Rapport R 86/3 de l'Ecole des Mines de Paris pour la CSMSE, unpublished, 1986 [in French].
[22] Bérest P, Blum PA, Charpentier JP, Gharbi H, Valès F. Very slow creep tests on rock samples. Int J Rock Mech Min Sci 2005;42: 569–76.
[23] Van Sambeek LL. Salt pillar design equation. In: Aubertin M, Hardy Jr HR, editors. Proceedings of the fourth conference on mechanical behavior of salt. Clausthal-Zellerfeld, Germany: Trans Tech Publishers; 1996. p. 495–508.
[24] Laouafa F, Ghoreychi M. Salt pillar creep analysis. In: Van Cotthem A, Charlier R, Thimus JF, Tshibangu JP, editors. Proceedings of the Eurock '06, Liège, Belgium. London: Taylor & Francis; 2006. p. 381–8.
[25] Salençon J, Matar M. Bearing capacity of axially symmetrical shallow foundations. (Capacité portante des fondations circulaires). J Méc Théor Appl 1982;1(2):237–67 [in French].
[26] Bhattacharya S, Singh MM, Chen CY. Proposed criteria for subsidence damage to buildings. In: Dowding CH, Singh MM, editors. Proceedings of the 25th symposium on rock mechanics. Soc Mining Eng AIME; 1984. p. 747–55.
[27] DeVries KL. Geomechanical analyses to determine the onset of dilation around natural gas storage caverns in bedded salt. In: Proceedings of the SMRI spring meeting, Brussels, 2005. p. 132–48.
[28] Spiers CJ, Peach CJ, Brzesowsky P, Liezenberg JL, Zwart HJ. Long-term rheological and transport properties of dry and wet salt rocks. Final Report, Nuc Sci Tech, Comm Eur Commun, EUR 11848 EN, 1989.
[29] Aubertin M, Sgaoula J, Gill DE. A damage model for rocksalt: application to tertiary creep. In: Kakinaha H, Hardy Jr HR, Hoshi T, Toyokura K, editors. Proceedings of the seventh symposium on salt, vol. 1. Amsterdam: Elsevier; 1993. p. 117–25.
[30] Van Sambeek L, Fossum A, Callahan G, Ratigan J. Salt mechanics: empirical and theoretical developments. In: Kakinaha H, Hardy Jr HR, Hoshi T, Toyokura K, editors. Proceedings of the seventh symposium on salt, vol. 1. Amsterdam: Elsevier; 1993. p. 127–34.
[31] Hunsche U. Determination of dilatancy boundary and damage up to failure for four types of rock salt at different stress geometries. In: Aubertin M, Hardy Jr HR, editors. Proceedings of the fourth conference on mechanical behavior of salt. Clausthal-Zellerfeld, Germany: Trans Tech Publishers; 1996. p. 163–74.
[32] Cristescu N, Hunsche U. A comprehensive constitutive equation for rock salt: determination and application. In: Hardy Jr RH, Langer M, editors. Proceedings of the third conference on the mechanical behavior of salt. Clausthal-Zellerfeld, Germany: Trans Tech Publishers; 1996. p. 191–205.
[33] Thorel L, Ghoreychi M. Rock salt damage—experimental results and interpretation. In: Hardy Jr RH, Langer M, editors. Proceedings of the third conference on the mechanical behavior of salt. Clausthal-Zellerfeld, Germany: Trans Tech Publishers; 1996. p. 175–89.
[34] Lux KH, Hou Z, Düsterloh U, Xie Z. Approaches for validation and application of a new material model for rock salt including structural damages. In: Geertman RM, editor. Proceedings of the eighth world salt symposium "Salt 2000," The Hague, vol. 1. Amsterdam: Elsevier; 2000. p. 271–7.
[35] Pfeifle TW, Hurtado LD. Effect of pore pressure on damage accumulation in salt. In: RM Geertman, editor. Proceedings of the eighth world salt symposium "Salt 2000," The Hague, vol. 1. Amsterdam: Elsevier; 2000. p. 307–12.
[36] Chan KS, Munson DE, Fossum AF, Bodner SR. A constitutive model for representing coupled creep, fracture and healing in rock salt. In: Aubertin M, Hardy Jr HR, editors. Proceedings of the fourth conference on mechanical behavior of salt. Clausthal-Zellerfeld, Germany: Trans Tech Publishers; 1996. p. 221–47.
[37] DeVries KL, Mellegard KD, Callahan GD. Cavern design using a salt damage criterion: proof-of-concept research final report. In: Proceedings of the SMRI spring meeting, Houston, 2003. p. 1–18.
[38] Rokahr R, Staudtmeister K, Zander-Schiebenhöfer D. Application of a continuum damage model for cavern design—case study: atmospheric pressure. In: Proceedings of the SMRI spring meeting, Wichita, Kansas, 2004. p. 38–55.
[39] Nieland JD, Ratigan JL. Geomechanical evaluation of two Gulf Coast natural gas Storage caverns. In: Proceedings of the SMRI spring meeting, Brussels, 2006. p. 61–89.
[40] Bauer SJ, Ehgartner BL, Neal JT. Geotechnical studies associated with decommissioning the Strategic Petroleum Reserve Facility at Weeks Island, Louisiana: a case history. In: Proceeding of the SMRI fall meeting, San Antonio, 2000. p. 145–56.